Development of real-time vibrational spectroscopy of molecules in electronic excited states: toward mapping molecular potential energy hypersurfaces

Takahiro Teramoto,[1,2,*] Juan Du,[1,2,3] Zhuan Wang,[1,2] Jun Liu,[1,2,3] Eiji Tokunaga,[4] and Takayoshi Kobayashi[1,2,3,5,6]

[1]*Advanced Ultrafast Laser Research Center and the Department of Engineering Science, Faculty of Informatics and Engineering, Department of Engineering Science, The University of Electro-Communications, 1-5-1, Chofugaoka, Chofu, Tokyo 182-8585, Japan*

[2]*International Cooperative Research Project (ICORP), Japan Science and Technology Agency, 4-1-8 Honcho, Kawaguchi, Saitama 332-0012, Japan*

[3]*Core Research for Evolutional Science and Technology (CREST), Japan Science and Technology Agency, 4-1-8 Honcho, Kawaguchi, Saitama 332-0012, Japan*

[4]*Department of Physics, Faculty of Science, Tokyo University of Science, Shinjuku Ku, Tokyo 1628601, Japan*

[5]*Department of Electrophysics, National Chiao Tung University, Hsinchu 30010, Taiwan*

[6]*Institute of Laser Engineering, Osaka University, 2-6 Yamada-oka, Suita, Osaka 565-0871, Japan*

*Corresponding author: teramoto@ils.uec.ac.jp

We have developed an experimental system for real-time vibrational spectroscopy of molecules in a specific electronic excited state. A synchronized UV light source and a few-cycle visible laser pulse were utilized to prepare and investigate the ultrafast dynamics of molecules in the electronic excited states. A multichannel lock-in amplifier detection system operating in a tandem double lock-in detection mode was used to extract the signal correlated only to the UV and visible pump pulses. Real-time vibrational spectroscopy of chrysene in the triplet state and 1′, 3′-dihydro-1′, 3′, 3′-trimethyl-6-nitrospiro [2H-1-benzopyran-2, 2′-(2H)-indole] in a photochromic state was demonstrated.   © 2011 Optical Society of America

OCIS codes: 320.7130, 320.7150, 300.6250.

1. INTRODUCTION

During the course of research into light–matter interactions in the time domain, real-time vibrational spectroscopy using ultrashort pulses has provided new insights into the ultrafast dynamics of molecules [1–31]. Real-time vibrational spectroscopy gives us the information of both the amplitude and phase of molecular vibration in addition to the relaxation dynamics of electronic excited states. The modulation of instantaneous vibrational frequency due to mode coupling can be detected by real-time vibrational spectroscopy, while femtosecond stimulated Raman spectroscopy [32–34], which is also time-domain spectroscopy, cannot resolve the modulation and nonstationary frequency in cases when the modulation period is *only* a few times greater than the carrier frequency. Studies in real-time vibrational spectroscopy have been developed to investigate the dynamic vibrational mode coupling in molecules [11,14–16,27]. Furthermore, study of vibronic coupling through real-time vibrational spectroscopy has shown the structural changes in molecules, including transition states and intermediates during photochemical reaction [22,25] and reaction even in the ground state [26]. The method is expected to provide information about potential hypersurfaces [18–21]. Self-trapped excitons in conjugated polymers with nondegenerate ground states and solitons in *trans*-polyacetylene have also been studied [11,24]. However, a limitation of real-time vibrational spectroscopy is that the target molecule is always initially in the electronic ground state.

To gain much broader insights into the electronic excited states and to control the molecular reactions, techniques such as pump–repump–probe and pump–dump–probe have been used [35,36]. However, these techniques also have a limitation in that the maximum time range is up to several nanoseconds due to the use of a single laser source and optical delay.

Long-time-range experiments from several nanoseconds to seconds have been performed using flash photolysis [37] but with low time resolutions. Recently, an attempt was made to construct an experimental setup that would extend the time range from femtoseconds to milliseconds [38,39]. These experimental techniques can be used to obtain the transient absorption spectra of electronic excited states. By applying long-time-range techniques to real-time vibrational spectroscopy, the ultrafast dynamics of molecules can be investigated based on the vibrational structure of different electronic excited states.

The few-cycle laser pulses used in real-time vibrational spectroscopy have a very broad bandwidth. Therefore, to fully utilize the available frequency information, a broadband detector is required that has both high resolution and high sensitivity. Our group previously reported an original detection system composed of a multichannel lock-in amplifier (MLA)

[40] and we demonstrated the advantages of this system by applying it to several samples [16–29,40]. Recently, several groups have utilized two-dimensional (2D) detectors, such as CCDs [41] and photodiode arrays [42]. However, these detection systems have limited dynamic ranges due to the background noise extending over the entire frequency region [43]. Thus, the reported absorbance change spectra measured by these detectors are usually on the order of 10^{-3} [44,45]. Such a noise effect is lower in our MLA system because the lock-in amplifier is just a filter circuit that extracts a specific frequency component.

In the present paper, we demonstrate a laser system based on synchronization between picosecond and femtosecond regenerative amplifiers. This synchronization is achieved by a phase-locked-loop system [38]. By combining a synchronized double-laser system with a MLA detection system, we can extend the real-time vibrational spectroscopy of molecules from the electronic ground state to the different excited states, with lifetimes of up to 1 ms after photoexcitation. The prerequisite of setting molecules in a specific electronic excited state is achieved by irradiating with a picosecond UV pulse that does not excite molecular vibrations. The visible femtosecond pump and probe pulses are irradiated to the molecules in the excited state, allowing real-time observation of molecular vibrations in specific electronic excited or intermediate states of photochemical reactions. A highly sensitive detector is required because excited or intermediate states have much smaller populations than the ground state. Additionally, the detector needs to be able to detect two different pump pulses. A double lock-in technique [44,45] is applied to the MLA system to extract the signal correlated with only UV and visible pump pulses. To demonstrate the benefits of our experimental setup (see Fig. 1), real-time vibrational spectroscopy of chrysene in the triplet state and a photochromic molecule was performed.

2. EXPERIMENTAL SETUP

A. Light Sources

1. Noncollinear Optical Parametric Amplifier

The pump source for the noncollinear optical parametric amplifier (NOPA) system [46,47] was a commercially available regenerative amplifier [48] that produces 35 fs pulses at a repetition rate of 1 kHz with a center wavelength of 790 nm and an average output power of 2.3 W. A small fraction of the fundamental beam was focused on a 2 mm thick $Y_3Al_5O_{12}$ plate [49] to generate a white light continuum through a single stable filament. The second harmonic (SH) was generated in a 0.4 mm thick β-BaB_2O_4 (BBO) crystal (type I, $\theta = 29.2°$) using a pulse with an energy of $25\,\mu J$. The SH was separated from the fundamental and was utilized as the pump for the NOPA system.

The external noncollinear angle between the pump beam and seed was $6.4°$ at the BBO crystal. This corresponds to an internal angle of $3.7°$, which allows broadband phase matching. After the double-pass NOPA, the amplified signal pulse had a spectrum extending from 1.69 to 2.37 eV (523–733 nm) and was first compressed by a pair of chirped mirrors and then by a pair of prisms. The final pulse duration was 6.2 fs, which is close to the Fourier-transform (FT) limit. The pulse from the NOPA was split into pump and probe pulses with energies of approximately 60 and 6 nJ, respectively.

2. UV Light Source

A picosecond regenerative amplifier system [48] was employed to electronically excite the target molecules without inducing molecular vibrations. The amplifier had a repetition rate of 1 kHz, producing 1 ps pulses with a center wavelength of 800 nm and an average output power of 1 W. The UV (400 nm or 266 nm) pulse was created via SH generation and third-harmonic generation in type I BBO crystals. In this study, we utilized only the wavelength of 266 nm. To avoid damaging the sample, the output power of the UV source (>30 mW) was attenuated to 1 mW so that the pump intensity at the sample surface was approximately $0.35\,TW/cm^2$.

3. Synchronization of NOPA and UV Light Sources

Synchronization of the two light sources was performed for both the oscillators and amplifiers. The phase-locked-loop system synchronized the femtosecond and picosecond oscillators, which were operated as the master and slave units, respectively [48]. The timing jitter was nominally lower than 200 fs, and the relative delay time range (the reciprocal of the oscillator repetition rate) was 13.2 ns. Synchronization of the amplifier systems was performed via a Countdown Electronics 76 MHz to 1 kHz unit, Q-switch timing of the pump lasers, and synchronization and delay generators (SDGs). The radio-frequency (76 MHz) signal from the femtosecond oscillator was connected to the Countdown Electronics 76 MHz to 1 kHz unit to generate a 1 kHz signal synchronized with the oscillator repetition rate. Digital function generators [48] guided the 1 kHz signal to the Q-switch timing system of the pump lasers and SDGs. The timing jitter between each output pulse of the regenerative amplifiers was determined to be 700 fs from a cross-correlation trace. The delay between the two pulses could be tuned from 0 ps to 1 ms (the reciprocal of the repetition rate of the regenerative amplifier system). The relative time delay between the femtosecond and picosecond regenerative amplifier systems was adjusted by varying the Q-switch timing of the pump lasers and the timing of the SDGs via a digital delay generator with a 13.2 ns coarse step and by changing the relative phase of the picosecond and femtosecond oscillators during precise tuning. The relative delay between the two pulses was measured by a p-i-n photodiode [48]. In the time scale less than the regenerative round trip time, we need to adjust the firing timing of the Q switch of the pump laser and the phase shift of the phase-locked-loop system simultaneously. To precisely lock both output pulses from the amplifiers, the phase-locked-loop system in the 2D IR experiment [50] may be beneficial. However, because the time range in this paper is on the order of nanoseconds, the timing jitter with less than 1 ps can be negligible.

B. Pump–Probe Setup

For the pump–probe experiment, the output beam from the NOPA, as described in Subsection 2.A.1, was divided into two and used for both the pump and probe. The pump–probe setup consisted of a two-arm delay line with a Michelson interferometer configuration (see the upper-right of Fig. 1). The probe pulse was perpendicular to the original beam after being reflected from a beam splitter, and it was guided to
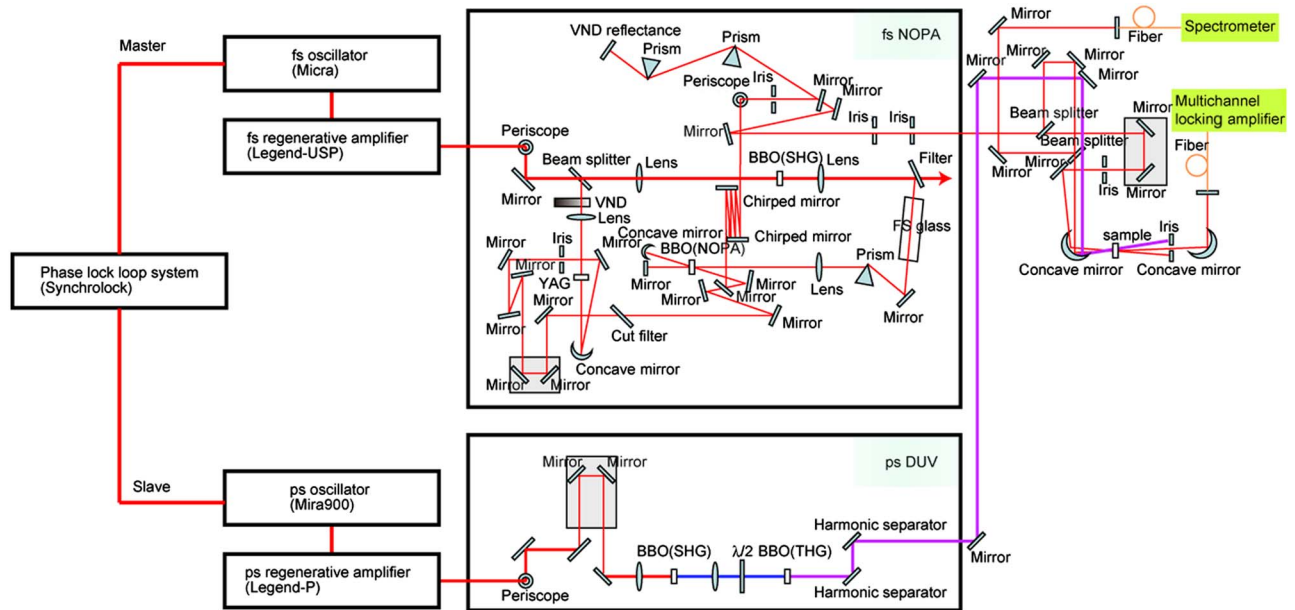
Fig. 1. (Color online) Schematic diagram of the experimental setup.

an off-axis parabolic mirror. The pump pulse that was transmitted to the beam splitter was retroreflected with an optical delay line and guided to an off-axis parabolic mirror that was parallel to the probe pulse. The optical delay of the pump pulse was tuned by a high-resolution, high-precision feedback stage [48]. The resolution of each stage step was up to 10 nm (0.03 fs), and the reproducibility accuracy was 20 nm due to the quartz scale and ball lead used to determine the position of the stage. The stage could be moved at a maximum speed of 10 mm/s. Both the pump and probe pulses were guided to off-axis parabolic mirrors and focused noncollinearly onto the sample stage with a relative angle of less than 3°. The pulses were characterized by the autocorrelation method using a 10 μm thick BBO crystal. The BBO crystal was placed at the focal point of both the pump and probe pulses, and the generated sum frequency component was detected by a photomultiplier.

In the pump–probe experiment, the BBO crystal used to characterize the pulses was replaced by the sample. The transmitted probe pulse was refocused onto a multimode fiber and guided to the detection system. In the NOPA pump–probe experiment without a picosecond UV pulse, the absorption difference spectrum was measured by placing an optical chopper [48] in the pump beam to detect the modulation induced in the probe pulse by the NOPA pump pulse.

For this study, we prepared an additional UV light source. UV light was guided collinearly and focused with the NOPA probe pulse. In the UV pump–NOPA probe experiment, the optical chopper was applied to the UV pump pulse. To achieve double modulation in the UV pump–NOPA pump–probe experiment, a shutter was placed in the UV beam and a chopper was placed in the NOPA pump beam. All modulated probe pulses were guided to the MLA system described in the following section. A signal with the same frequency as the modulation frequency was demodulated by applying the transistor–transistor–logic signal produced using the chopper or shutter whose modulation frequency was used as the reference frequency for the MLA.

C. Detection System
1. Multichannel Lock-in Amplifier System
The MLA system has previously been outlined in [40]. Here, we describe improvements we have made to the system.

Our modified detection system included a multimode fiber, a polychromator, a 128-channel fiber bundle array, 128 Si avalanche photodiodes (APDs), 128 preamplifiers, 128 active low-pass filters produced in house, and four 32-channel lock-in amplifiers [48].

The NOPA probe beam was guided to the polychromator by the multimode fiber. Light dispersed by the polychromator was coupled into the 128-channel fiber bundle array placed in the focal plane of the polychromator. To acquire a high photon flux, this 2D fiber array was composed of 128 rows and 16 columns. On the other side of the fiber array, every 16 fibers were bundled into a single fiber. Thus, a broad frequency range could be registered by the 128 independent fibers. The spectral resolution and spectral coverage depend on the groove number of the grating and slit width of the input side in the polychromator. Because, in the present experiment we selected the grating with 300 grooves/mm, the detected spectra bandwidth was 180 nm. This allowed the entire spectral range of the NOPA probe pulse to be detected simultaneously with a resolution of 1 nm.

The 128 fibers were guided to corresponding 128-channel Si APDs and preamplifiers. The Gaussian-like output signal from the preamplifier contained high-frequency components, even after dispersion by the polychromator grating because of the short probe pulse duration (<10 fs). To reduce unwanted higher harmonic frequency components, an active low-pass filter kit was included in the MLA system. Figure 2 shows a schematic diagram of the low-pass filter. Its cutoff frequency can be controlled by varying the external resistance. For our laser system, the 1 kHz repetition rate means that the maximum modulation frequency of the pump pulse is 0.5 kHz. As shown in Fig. 2, the filter can reduce the fundamental component by 40 dB without reducing the modulation frequency component. This was possible because the cutoff frequency of the filter was designed to be 1.2 times greater than the maximum
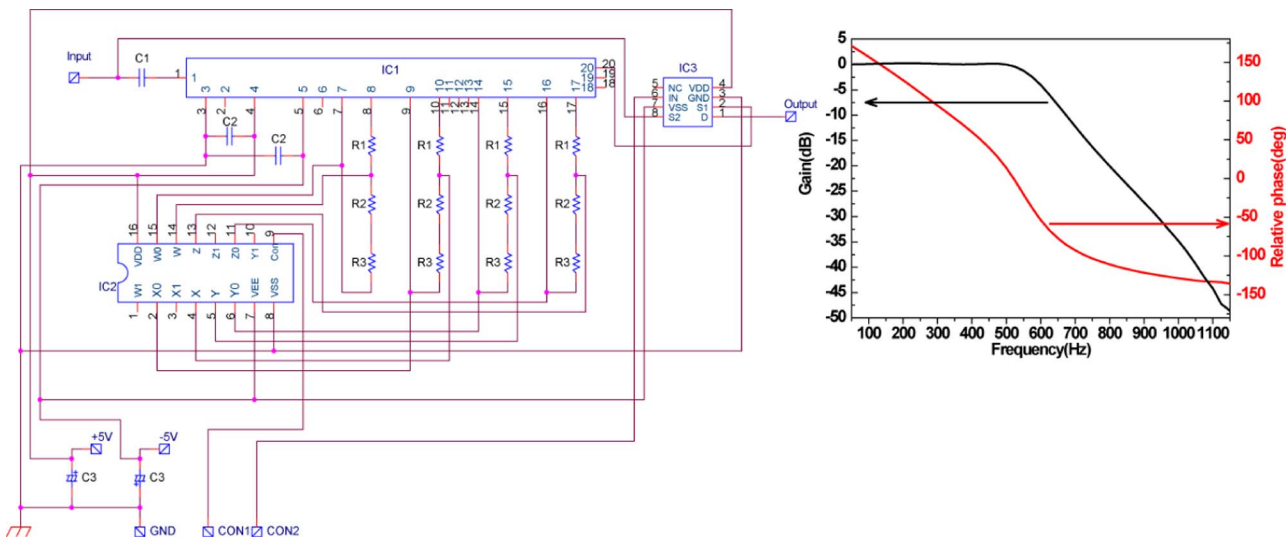
Fig. 2.   (Color online) Schematic diagram of the low-pass filter kit: R1, 56 Ωk; R2, 200 Ωk; R3, 13 Ωk; C1, 4.7 μF; C1, 0.1 μF; C3, 10 μF; IC1, SR-4FL2; IC2, MC14551BD; IC3, ADG619. Con1; selection switch for the cutoff frequency (0.6 or 3 kHz); Con2, selection switch for the application of the low-pass filter to the input signal. The graph (right) shows the frequency response of the filter.

modulation frequency. As shown in Fig. 2, the filter kit has two control switches: one switch guides the input signal, with or without the application of the low-pass filter, to the output, while the other switch selects the cutoff frequency as either 0.6 or 3 kHz (for the laser system with a repetition rate of 5 kHz).

In our experimental setup, we connected four 7210 lock-in amplifiers together to form a single system ($32 \times 4 = 128$ total channels). The noise level at 1 kHz was $50 \, \text{fA}/\sqrt{\text{Hz}}$, and it was possible to detect very weak signals in the pump–probe experiments, as demonstrated in Subsection 3.A.2. The lock-in system detects only signals with the same frequency and phase as the reference signal. Consequently, the MLA, in principle, offers a higher sensitivity than other 2D detectors, such as CCD cameras and photodiode arrays. An example of the high sensitivity of this system for absorbance change spectra measurement has been presented in Ref. [45].

2. Tandem Double Lock-in Detection

For the regular pump–probe experiment, the modulation frequency of the probe pulse corresponds to the chopped pump pulse. If we guide the probe pulse to the lock-in amplifier, the reference frequency (corresponding to the modulation frequency of the pump pulse) is needed to extract the difference between the signals with and without the pump pulse. The lock-in amplifier acts as a filter circuit and demodulates the signal with the same frequency as the reference frequency. However, the UV picosecond pump–NOPA femtosecond pump–NOPA femtosecond probe experiment requires two different modulation frequencies and detection systems to extract the signal that correlates to just the two pump pulses. We introduced tandem double lock-in detection for this purpose.

The signal component to be extracted can be described as follows:

$$\Delta \Delta T = \left\{ \begin{pmatrix} \text{UVpumpON} \\ \text{NOPApumpON} \end{pmatrix} - \begin{pmatrix} \text{UVpumpON} \\ \text{NOPApumpOFF} \end{pmatrix} \right\} \\ - \left\{ \begin{pmatrix} \text{UVpumpOFF} \\ \text{NOPApumpON} \end{pmatrix} - \begin{pmatrix} \text{UVpumpOFF} \\ \text{NOPApumpOFF} \end{pmatrix} \right\}. \quad (1)$$

When the probe pulse is guided to the first lock-in amplifier and the reference frequency is selected to be the same as the frequency of the NOPA pump pulse, the signal registered by the lock-in amplifier has two different components: one with and one without the UV pump pulse. Then, if the resultant signal is guided to the next lock-in amplifier and the reference frequency is set to the frequency of the UV pump pulse, the output signal of this lock-in amplifier correlates only to the two pump pulses. This double lock-in scheme is encompassed by the digital signal processor of the MLA system.

To acquire a signal with a maximum height, the relationship between the time constant and the modulation frequency should be expressed as follows [44,45]:

$$f_2 \tau_1 = 1, \quad (2)$$

where f_2 is the second modulation frequency and τ_1 is the time constant of the first lock-in detection system. In this study, we selected f_2 and τ_1 to be 1 Hz and 1 s, respectively. Because the lock-in amplifier is simply considered to be a frequency filter, the time constant of the low-pass filter in the lock-in amplifier limits the signal-to-noise ratio. Thus, the longer time constant provides us a better resolution signal, in principle. In Ref. [45], the authors selected the time constant as 50 min. Thus, they can get the absorbance change spectra with an order of 10^{-6}. However, it takes a very long time to acquire the data, because it needs at least about three times of the time constant of the low-pass filter in the measurement by using the lock-in amplifier. In ultrafast spectroscopy, instability of output power from a laser in use during data acquisition time limits the setting of the long time constant. Considering the trade-off between stability and the averaging time, the time constant of the second lock-in detection was determined to be 3 s in the present experiment. As shown in Section 3, the limitation of the detectable absorbance difference was $\sim 10^{-5}$.

D. Samples

The test samples for the experimental system were chrysene (Sigma-Aldrich, Inc.) and 1′, 3′-dihydro-1′, 3′, 3′-trimethyl-6-nitrospiro [2H-1-benzopyran-2, 2′-(2H)-indole] (6-nitro-BIPS) (Tokyo Chemical Industry, Inc.). They were used without
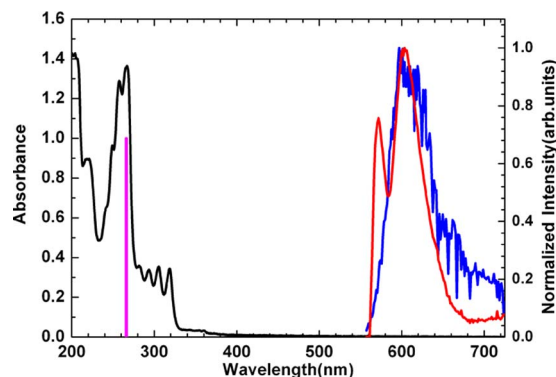
Fig. 3. (Color online) Stationary (black curve) and triplet–triplet (T–T) absorption spectra of chrysene (red curve). Laser spectral profiles for the UV (violet line) and NOPA pulse (blue curve). The T–T absorption spectra were measured by NOPA pulse irradiation 100 ns after the UV pulse.

further purification. The chrysene was dissolved in hexane, and the 6-nitro-BIPS was dissolved in toluene. The sample solutions were kept in a quartz cell with an optical path length of 1 mm during the experiment.

3. REAL-TIME VIBRATIONAL SPECTROSCOPY OF MOLECULES IN ELECTRONIC EXCITED STATES

A. Chrysene Molecules in the Triplet State
Chrysene is one of most extensively studied molecules by absorption, emission, and Raman spectroscopies [51–53]. Thus, its properties are well known; it has an S_1 lifetime of 40 ns and an intersystem crossing quantum efficiency of greater than 0.81 [52]. As shown in Fig. 3, the stationary absorption spectrum for the singlet state shows absorption in the UV range but no absorption in the visible range.

1. UV Picosecond Pump–NOPA Probe Experiment
If we use the UV (266 nm) picosecond light source to generate the pump pulse and the NOPA to produce the probe pulse, we can study transient absorption in the absence of molecular vibrations with the MLA system in single lock-in mode. Figure 3 shows the UV and NOPA laser spectra that were utilized in this experiment.

The red curve in Fig. 3 indicates the transient absorption spectrum of the chrysene molecules in the triplet state. As noted in Subsection 2.A.3, the relative delay time between the UV picosecond pulse and the NOPA pulse can be tuned between 0 ps and 1 ms; here, the time delay between the UV pump and NOPA probe pulses was set to 100 ns. The energies of these irradiation pulses were 1 μJ and 6 nJ, respectively. The pulse beam diameters at the sample were measured by a beam profiler to be 600 and 700 μm, respectively. To prepare and probe only molecules in the triplet state, both the diameter and intensity of the UV pump pulse needed to be greater than those of the NOPA probe pulse.

2. UV Picosecond Pump–NOPA Femtosecond Pump–NOPA Femtosecond Probe Experiment
Under the same experimental conditions, we introduced a NOPA pump pulse (energy, 60 nJ; diameter at the focal point, 100 μm) to investigate the dynamics of the chrysene molecules in the triplet state.

For this experiment, the NOPA pump pulse was chopped by an optical sector, and the UV pump pulse was chopped by an optical shutter to generate double modulation of the NOPA probe pulse. The modulation frequencies were 500 and 1 Hz, respectively. The MLA system was operated in the tandem double lock-in mode. Real-time vibrational spectroscopy of the chrysene molecules in the triplet state was performed for delay times of –100 to 700 fs in 1 fs steps.

Figure 4(a) shows the 2D absorbance change spectra [$\Delta\Delta A(\omega, t) = -\log(1 + \Delta\Delta T/T)$]. Figure 4(b) shows the probe delay dependence of $\Delta\Delta A$ for the relaxation of the electronic excited state with molecular vibration. Strong photobleaching is observed in the region from 540 to 580 nm, and weakly induced absorption spectra appear between 600 and 660 nm. Although $\Delta\Delta A$ is very small [$\sim 10^{-5}$; see Fig. 4(c)], the $\Delta\Delta A$ signal can be acquired without difficulty due to the high sensitivity of the lock-in amplifier.

B. Photochromic 6-Nitro-BIPS
Photochromic molecules have been extensively investigated for several decades [54], because they can be used for photoswitches [55,56] and 3D memory [57]. When a photochromic molecule is irradiated by UV light, absorption is shifted to a longer wavelength due to structural changes in the molecule,
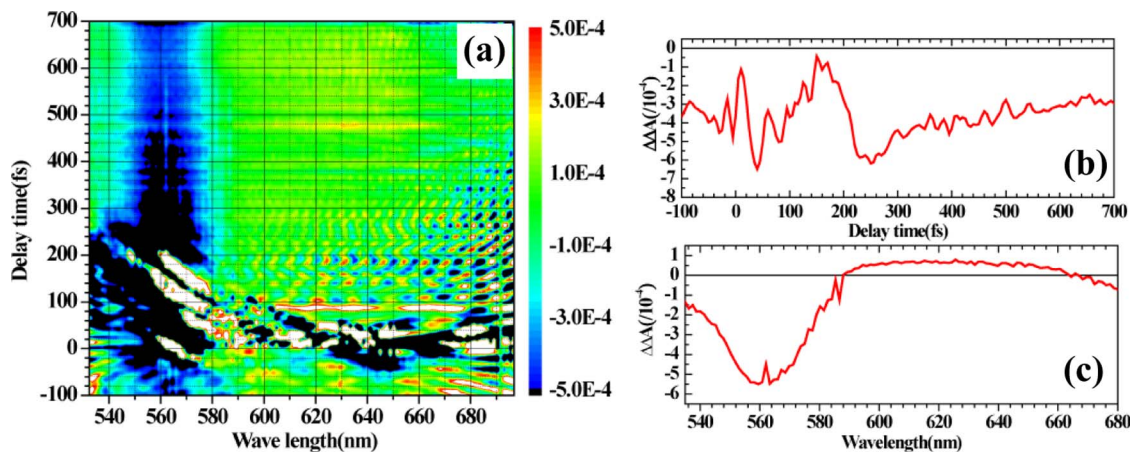
Fig. 4. (Color online) (a) 2D plot of $\Delta\Delta A(\omega, t)$ of chrysene in the triplet state. The contour means the intensity from –0.0005 (blue) to 0.0005 (red). (b) Integrated real-time traces of $\Delta\Delta A(\omega, t)$ for the wavelength range of 540 to 580 nm. (c) $\Delta\Delta A(\omega, t)$ as a function of wavelength at a delay time of 300 fs.
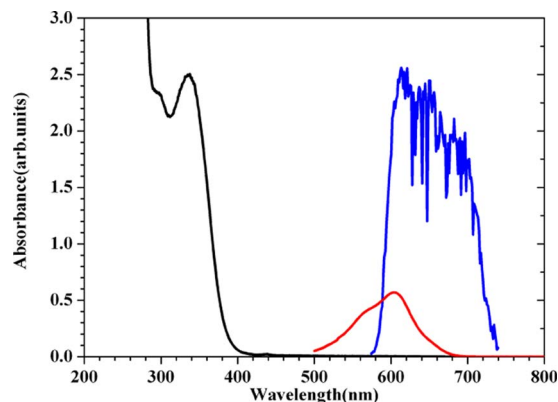
Fig. 5.   (Color online) Stationary absorption spectra before (black curve) and after (red curve) UV irradiation of 6-nitro-BIPS. The NOPA pulse profile is also shown (blue curve).

such as photoisomerization and ring-opening reactions [54]. 6-nitro-BIPS is a photochromic molecule that exhibits the ring-opening reaction most clearly [58–60]. UV irradiation opens the ring, and 6-nitro-BIPS becomes a merocyanine molecule. Here we use our experimental system to investigate the ultrafast dynamics of merocyanine (6-nitro-BIPS in the excited state).

Figure 5 shows the stationary absorption spectra. Before UV irradiation, there is no absorption in the visible region, whereas after UV irradiation, absorption appears in the visible region (indicated by the red curve in Fig. 5). Because the lifetime of the excited 6-nitro-BIPS molecule ($>1\,\mathrm{s}$) is longer than the repetition rate of the laser system, a higher absorption density can be achieved than for chrysene. Thus, we may regard the excited 6-nitro-BIPS molecule as a pure material, in the same way as in a conventional NOPA pump–probe experiment.

Figure 6 shows the 2D absorbance change spectra [$\Delta\Delta A(\omega,t)$] of the spiropyran-derived merocyanine. The strong absorption that appears around $590\,\mathrm{nm}$ is due to bleaching/induced emission with a periodic modulation due to molecular vibration. Figure 7 shows the FT of the $\Delta\Delta A(\omega,t)$ spectra. The intense signals at 521, 789, 1009, and $1217\,\mathrm{cm}^{-1}$ are due to the solvent toluene of the 6-nitro-BIPS solution sample. Others are due to the 6-nitro-BIPS. The components at 941, 1165, 1209, 1246, and $1393\,\mathrm{cm}^{-1}$ are attributed to merocyanine molecules based on theoretical calculation
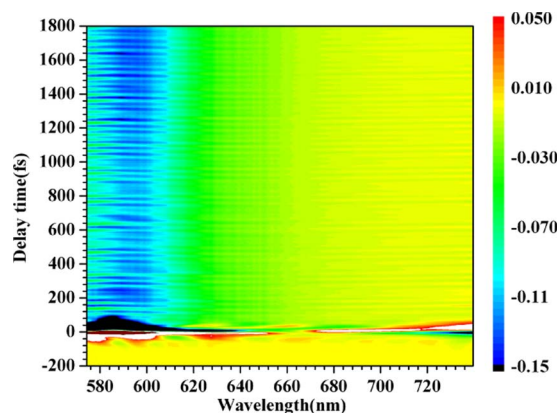
Fig. 6.   (Color online) 2D plot of $\Delta\Delta A(\omega,t)$ of 6-nitro-BIPS after UV irradiation. Contour means the intensity from –0.15 (blue) to 0.05 (red).
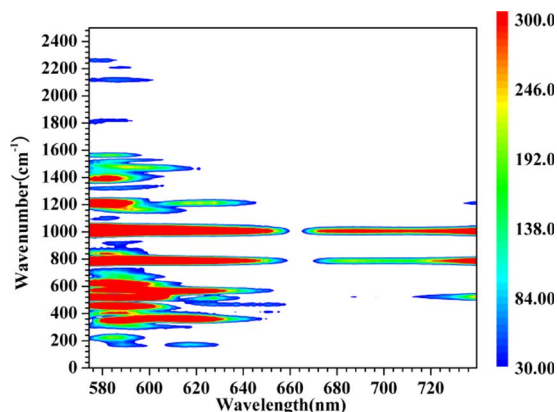
Fig. 7.   (Color online) Fast FT spectra of $\Delta\Delta A(\omega,t)$ of 6-nitro-BIPS after UV irradiation.

[58]. A more detailed discussion will be presented elsewhere soon.

4. CONCLUSION

We have developed a new experimental system for real-time vibrational spectroscopy to investigate molecules in the excited, intermediate, and transition states. This system has the many following advantages:

1.   A UV picosecond pulse excites the molecule into an electronic excited state or a few states without inducing molecular vibrations.

2.   The NOPA pump pulse generates signals due to induced absorption, stimulated emission, and bleaching coupled to molecular vibrations excited impulsively.

3.   Because of the broadness of the NOPA probe pulse, the wavelength dependence of the absorbance change induced by wave packet dynamics can be investigated to obtain detailed information concerning vibronic interactions and mode coupling.

4.   Because the UV and NOPA pulses are synchronized, the time delay between the pulses can be tuned easily between 0 and 1 ms. Thus, we can select molecules in specific electronic excited states after photoexcitation.

5.   The MLA system is a powerful tool for investigating wave packet dynamics with high sensitivity. Additionally, by applying the tandem double lock-in technique, we can extract signals correlated only to the double modulation.

By utilizing this spectroscopic technique, we can investigate a wide range of molecules in specific electronic excited states. The final goal of using this experimental system is the investigation of the whole chemical reaction processes initiated by the laser pulse including the transition states, intermediate states, and final products. Recently, with the aid of progress in computational technology, quantum chemical approaches, such as the time-dependent Hartree–Fock calculations, have also been implemented [36,61,62]. The experimental evidences of this system helps the theoretical technique and gives us the interpretation of the dynamics by mapping the molecular potential energy hypersurfaces [18–20].

REFERENCES AND NOTES

1. Y. R. Shen, *The Principles of Nonlinear Optics* (Wiley-Interscience, 1984).
2. J. Chesnoy and A. Mokhtari, "Resonant impulsive-stimulated Raman scattering on malachite green," Phys. Rev. A **38**, 3566–3576 (1988).
3. L. Dhar, J. A. Rogers, and K. A. Nelson, "Time-resolved vibrational spectroscopy in the impulsive limit," Chem. Rev. **94**, 157–193 (1994).
4. D. M. Jonas, S. E. Bradforth, S. A. Passino, and G. R. Fleming, "Femtosecond wavepacket spectroscopy: influence of temperature, wavelength, and pulse duration," J. Phys. Chem. **99**, 2594–2608 (1995).
5. S. Mukamel, *Principles of Nonlinear Optical Spectroscopy* (Oxford University Press, 1995).
6. L. Zhu, A. Widom, and P. M. Champion, "A multidimensional Landau–Zener description of chemical reaction dynamics and vibrational coherence," J. Chem. Phys. **107**, 2859–2871 (1997).
7. W. T. Pollard, S. L. Dexheimer, Q. Wang, L. A. Peteanu, C. V. Shank, and R. A. Mathies, "Theory of dynamic absorption spectroscopy of nonstationary states. 4. application to 12 fs resonant impulsive Raman spectroscopy of bacteriorhodopsin," J. Phys. Chem. **96**, 6147–6158 (1997).
8. S. Lochbrunner, A. J. Wurzer, and E. Riedle, "Ultrafast excited-state proton transfer and subsequent coherent skeletal motion of 2-(2′-hydroxyphenyl) benzothiazole," J. Chem. Phys. **112**, 10699–10702 (2000).
9. A. T. N. Kumar, F. Rosca, A. Widom, and P. M. Champion, "Investigations of ultrafast nuclear response induced by resonant and nonresonant laser pulses," J. Chem. Phys. **114**, 701–724 (2001).
10. A. T. N. Kumar, F. Rosca, A. Widom, and P. M. Champion, "Investigations of ultrafast nuclear response induced by resonant and nonresonant laser pulses," J. Chem. Phys. **114**, 6795–6815 (2001).
11. S. Adachi, V. M. Kobryanskii, and T. Kobayashi, "Excitation of a breather mode of bound soliton pairs in polymers with degenerate ground state by sub-5 fs optical pulses," Phys. Rev. Lett. **89**, 027401 (2002).
12. K. Heyne, N. Huse, J. Dreyer, E. T. J. Nibbering, and T. Elsaesser, "Coherent low-frequency motions of hydrogen bonded acetic acid dimers in the liquid phase," J. Chem. Phys. **121**, 902–913 (2004).
13. P. M. Champion, F. Rosca, D. Ionascu, W. Cao, and X. Ye, "Rapid timescale processes and the role of electronic surface coupling in the photolysis of diatomic ligands from heme proteins," Faraday Disc. **127**, 123–135 (2004).
14. J. R. Dwyer, J. Dreyer, E. T. J. Nibbering, and T. Elsaesser, "Ultrafast dynamics of vibrational N–H stretching excitations in the 7-azaindole dimer," Chem. Phys. Lett. **432**, 146–151 (2006).
15. T. Elsaesser, N. Huse, J. Dreyer, J. R. Dwyer, K. Heyne, and E. T. J. Nibbering, "Ultrafast vibrational dynamics and anharmonic couplings of hydrogen-bonded dimers in solution," Chem. Phys. **341**, 175–188 (2007).
16. T. Kobayashi, Y. Wang, Z. Wang, and I. Iwakura, "Circa conservation of vibrational energy among three strongly coupled modes of a cyanine dye molecule studied by quantum-beat spectroscopy with a 7 fs laser," Chem. Phys. Lett. **466**, 50–55 (2008).
17. T. Kobayashi, J. Du, W. Feng, and K. Yoshino, "Excited-state molecular vibration observed for a probe pulse preceding the pump pulse by real-time optical spectroscopy," Phys. Rev. Lett. **101**, 037402 (2008).
18. T. Kobayashi, Z. Wang, and I. Iwakura, "The relation between the symmetry of vibrational modes and the potential curve displacement associated with electronic transition studied by using real-time vibrational spectroscopy," New J. Phys. **10**, 065009 (2008).
19. T. Kobayashi and Z. Wang, "Correlations of instantaneous transition energy and intensity of absorption peaks during molecular vibration: toward potential hyper-surface," New J. Phys. **10**, 065015 (2008).
20. T. Kobayashi and Z. Wang, "Spectral oscillation in optical frequency-resolved quantum-beat spectroscopy with a few-cycle pulse laser," IEEE J. Quantum Electron. **44**, 1232–1241 (2008).
21. I. Iwakura, A. Yabushita, and T. Kobayashi, "Direct observation of molecular structural change during intersystem crossing by real-time spectroscopy with a few optical cycle laser," Inorg. Chem. **48**, 3523–3528 (2009).
22. I. Iwakura, A. Yabushita, and T. Kobayashi, "Why is indigo photostable over extremely long periods?" Chem. Lett. **38**, 1020–1021 (2009).
23. T. Kobayashi, J. Zhang, and Z. Wang, "Non-Condon vibronic coupling of coherent molecular vibration in MEH-PPV induced by a visible few-cycle pulse laser," New J. Phys. **11**, 013048 (2009).
24. T. Teramoto, Z. Wang, V. M. Kobryanskii, T. Taneichi, and T. Kobayashi, "Ultrafast real-time vibronic coupling of a breather soliton in *trans*-polyacetylene using a laser pulse with few cycles," Phys. Rev. B **79**, 033202 (2009).
25. I. Iwakura, A. Yabushita, and T. Kobayashi, "Kinetic isotope effect on the proton-transfer in indigo carmine," Chem. Phys. Lett. **484**, 354–357 (2010).
26. I. Iwakura, A. Yabushita, and T. Kobayashi, "Observation of transition state in Raman triggered oxidation of chloroform in the ground state by real-time vibrational spectroscopy," Chem. Phys. Lett. **457**, 421–426 (2008).
27. T. Teramoto and T. Kobayashi, "Multiple mode coupling in Cy3 molecules by impulsive coherent vibrational spectroscopy using a few-cycle laser pulse," Phys. Chem. Chem. Phys. **12**, 13515–13518 (2010).
28. Y. Wang and T. Kobayashi, "Electronic and vibrational coherence dynamics in a cyanine dye studied using a few cycles pulsed laser," Chem. Phys. Chem. **11**, 889–896 (2010).
29. T. Kobayashi, J. Du, W. Feng, K. Yoshino, S. Tretiak, A. Saxena, and Alan R. Bishop, "Observation of breather excitons and soliton in a substituted polythiophene with a degenerate ground state," Phys. Rev. B **81**, 075205 (2010).
30. C. Gadermaier, A. S. Alexandrov, V. V. Kabanov, P. Kusar, T. Mertelj, X. Yao, C. Manzoni, D. Brida, G. Cerullo, and D. Mihailovic, "Electron-phonon coupling in high-temperature cuprate superconductors determined from electron relaxation rates," Phys. Rev. Lett. **105**, 257001 (2010).
31. T. Virgili, L. Lüer, G. Cerullo, G. Lanzani, S. Stagira, D. Coles, A. J. H. M. Meijer, and D. G. Lidzey, "Role of intramolecular dynamics on intermolecular coupling in cyanine dye," Phys. Rev. B **81**, 125317 (2010).
32. M. Yoshizawa, Y. Hattori, and T. Kobayashi, "Femtosecond time-resolved resonance Raman gain spectroscopy in polydiacetylene," Phys. Rev. B **49**, 13259–13262 (1994).
33. M. Yoshizawa and M. Kurosawa, "Femtosecond time-resolved Raman spectroscopy using stimulated Raman scattering," Phys. Rev. A **61**, 013808 (1999).
34. C. Fang, R. R. Frontiera, R. Tran, and R. A. Mathies, "Mapping GFP structure evolution during proton transfer with femtosecond Raman spectroscopy," Nature **462**, 200–205 (2009).
35. D. S. Larsen, E. Papagiannakis, I. H. M. van Stokkum, M. Vengris, J. T. M. Kennis, and R. van Grondelle, "Excited state dynamics of beta-carotene explored with dispersed multi-pulse transient absorption," Chem. Phys. Lett. **381**, 733–742 (2003).
36. S. Takeuchi, S. Ruhman, T. Tsuneda, M. Chiba, T. Taketsugu, and T. Tahara, "Spectroscopic tracking of structural evolution in ultrafast stilbene photoisomerization," Science **322**, 1073–1077 (2008).
37. W. D. Tian, J. T. Sage, V. Srajer, and P. M. Champion, "Relaxation dynamics of myoglobin in solution," Phys. Rev. Lett. **68**, 408–411 (1992).

38. A. Yu, X. Ye, D. Ionascu, W. Cao, and P. M. Champion, "Two-color pump-probe laser spectroscopy instrument with picosecond time-resolved electronic delay and extended scan range," Rev. Sci. Instrum. **76**, 114301 (2005).

39. E. C. Carroll, M. P. Hill, D. Madsen, K. R. Malley, and D. S. Larsen, "A single source femtosecond–millisecond broadband spectrometer," Rev. Sci. Instrum. **80**, 026102 (2009).

40. N. Ishii, E. Tokunaga, S. Adachi, T. Kimura, H. Matsuda, and T. Kobayashi, "Optical frequency- and vibrational time-resolved two-dimensional spectroscopy by real-time impulsive resonant coherent Raman scattering in polydiacetylene," Phys. Rev. A **70**, 023811 (2004).

41. U. Megerle, I. Pugliesi, C. Schriever, C. F. Sailer, and E. Riedle, "Sub-50 fs broadband absorption spectroscopy with tunable excitation: putting the analysis of ultrafast molecular dynamics on solid ground," Appl. Phys. B **96**, 215–231 (2009).

42. D. Polli, L. Lüer, and G. Cerullo, "High-time-resolution pump-probe system with broadband detection for the study of time-domain vibrational dynamics," Rev. Sci. Instrum. **78**, 103108 (2007).

43. K. E. H. Anderson, S. L. Sewall, R. R. Cooney, and P. Kambhampati, "Noise analysis and noise reduction methods in kilohertz pump-probe experiments," Rev. Sci. Instrum. **78**, 073101 (2007).

44. J. Goree, "Double lock-in detection for recovering weak coherent radio frequency signals," Rev. Sci. Instrum. **56**, 1662–1664 (1985).

45. S. Iwai, M. Tanaka, M. Mitsunaga, T. Kobayashi, and E. Tokunaga, "Excited-state absorption spectra for optically forbidden f–f transitions in an $Eu^{3+}:Y_2SiO_5$ crystal and Eu^{3+} aqueous solution," J. Opt. Soc. Am. B **25**, 1046–1050 (2008).

46. A. Shirakawa, I. Sakane, and T. Kobayashi, "Pulse-front-matched optical parametric amplification for sub-10 fs pulse generation tunable in the visible and near infrared," Opt. Lett. **23**, 1292–1294 (1998).

47. A. Baltuska, T. Fuji, and T. Kobayashi, "Visible pulse compression to 4 fs by optical parametric amplification and programmable dispersion control," Opt. Lett. **27**, 306–308 (2002).

48. The double-laser systems were composed of a femtosecond regenerative amplifier system (Legend-USP, Coherent, Inc.) and a picosecond regenerative amplifier system (Legend-P, Coherent, Inc.). The timing firing the Q switch and SDG was tuned by the digital delay generator (DG535, Stanford Research). The timing signal was detected by the FPD-510-FV (Menlo Systems, Inc.) The feedback stage (FS-1020X, Sigma Tech, Inc.) was used to tune the pump's optical delay. The modulation for the probe pulse was created by the chopper (Model 3501, New Focus, Inc.) and shutter (SH05, Thorlabs, Inc.). The MLA system was composed of fibers (FiberTech Optica, Inc.), a polychromator (SpectraPro2300i, Acton Research, Inc.), APDs (S5343,

Hamamatsu Photonics, Inc.), preamplifier (7210/90, Signal Recovery, Inc.), and an MLA (7210, Signal Recovery, Inc.). The resistor tunable low-pass filter kit was used to reduce the unwanted higher frequency components of the signal (SR-4FL2, NF Corporation, Inc.).

49. M. Bradler, P. Baum, and E. Riedle, "Femtosecond continuum generation in bulk laser host materials with sub-μJ pump pulses," Appl. Phys. B **97**, 561–574 (2009).

50. V. Volkov, R. Schanz, and P. Hamm, "Active phase stabilization in Fourier-transform two-dimensional infrared spectroscopy," Opt. Lett. **30**, 2010–2012 (2005).

51. S. Koshihara and T. Kobayashi, "Time-resolved resonance Raman spectrum of chrysene in the S_1 and T_1 states," J. Chem. Phys. **85**, 1211–1219 (1986).

52. S. Koshihara, T. Kobayashi, and S. Iwashima, "$S_n \leftarrow S_1$ and $T_n \leftarrow T_1$ absorption spectra of highly purified chrysene in solution," Chem. Phys. Lett. **124**, 331–335 (1986).

53. X. Cai, M. Hara, K. Kawai, S. Tojo, and T. Majima, "Properties of chrysene in the higher triplet excited state," Chem. Phys. Lett. **368**, 365–369 (2003).

54. G. H. Brown, *Photochromism* (Wiley-Interscience, 1971).

55. M. Irie, "Diarylethenes for memories and switches," Chem. Rev. **100**, 1685–1716 (2000).

56. G. Berkovic, V. Krongauz, and V. Weiss, "Spiropyrans and spirooxazines for memories and switches," Chem. Rev. **100**, 1741–1753 (2000).

57. S. Kawata and Y. Kawata, "Three-dimensional optical data storage using photochromic materials," Chem. Rev. **100**, 1777–1788 (2000).

58. Y. Futami, M. Lim, S. Chin, S. Kudoh, M. Takayanagi, and M. Nakata, "Conformations of nitro-substituted spiropyran and merocyanine studied by low-temperature matrix-isolation infrared spectroscopy and density-functional-theory calculation," Chem. Phys. Lett. **370**, 460–468 (2003).

59. C. J. Wohl and D. Kuciauskas, "Excited-state dynamics of spiropyran-derived merocyanine isomers," J. Phys. Chem. B **109**, 22186–22191 (2005).

60. S. Kajimoto, A. Mori, and H. Fukumura, "Photo-controlled phase separation and mixing of a mixture of water and 2-butoxyethanol caused by photochromic isomerisation of spiropyran," Photochem. Photobiol. Sci. **9**, 208–210 (2010).

61. S. Tretiak, A. Piryatinski, A. Saxena, R. L. Martin, and A. R. Bishop, "On the existence of photoexcited breathers in conducting polymers," Phys. Rev. B **70**, 233203 (2004).

62. S. Tretiak, A. Saxena, R. L. Martin, and A. R. Bishop, "Photoexcited breathers in conjugated polyenes: an excited-state molecular dynamics study," Proc. Natl. Acad. Sci. USA **100**, 2185–2190 (2003).